

## IMPROVING SENSITIVITY OF $\text{In}_2\text{O}_3$ AGAINST $\text{NO}_2$ TOXIC GAS BY LOADING TIN OXIDE

I.M. IBRAHIM<sup>a</sup>, M. A. SALIM<sup>b</sup>, M. A. IFTIKHAR<sup>a</sup>

<sup>a</sup>*Department of physics ,College of, University of Baghdad , Baghdad, Iraq*

<sup>b</sup>*Department of energy engineering ,College of engineering, University of Baghdad , Baghdad, Iraq*

The paper discusses the structural and optical properties of  $\text{In}_2\text{O}_3$  and  $\text{In}_2\text{O}_3\text{-SnO}_2$  gas sensor thin films were deposited on glass and silicon substrates and grown by irradiation of assistant microwave on seeded layer nucleated using spin coating technique. The X-ray diffraction revealed a polycrystalline nature of the cubic structure. Atomic Force Microscopy (AFM) used for morphology analysis that shown the grain size of the prepared thin film is less than 100 nm, surface roughness and root mean square for  $\text{In}_2\text{O}_3$  where increased after loading  $\text{SnO}_2$ , this addition is a challenge in gas sensing application. Sensitivity of  $\text{In}_2\text{O}_3$  thin film against  $\text{NO}_2$  toxic gas is 35% at 300°C. Sensing properties were improved after adding Tin Oxide ( $\text{SnO}_2$ ) to be more than 800% at 200°C. So, higher sensitivity with lowering operating temperature is obtained by  $\text{SnO}_2$  addition. The results revealed fast response and recovery times with increasing operating temperatures.

(Received December 31, 2018; Accepted April 30, 2019)

*Keywords:*  $\text{In}_2\text{O}_3$ ,  $\text{SnO}_2$ , Spin coating, Seed layer, Microwave irradiation, Gas sensor

### 1. Introduction

In recent years, the development of high performance solid state chemical sensors is important in many advanced technological fields [1]. Previous researches have demonstrated that a characteristic of solid-state gas sensors was the reversible interaction of the gas with the surface of a solid-state material. Beside of the conductivity change of gas-sensing material, which can be detected by measuring the change of capacitance, work function, mass, optical characteristics or reaction energy released by the gas/solid interaction[2,3].

Another important task in environmental chemistry were represented by gaseous chemical detection and treatment [4-6]. The development of gas sensor and catalytic converter for environmental monitoring and remediation played a critical role in public health and safety [7], household security [8], automobile design [9] and defense technology [10]. Although that the materials selection and the device configuration might vary from case to case toward different applications, the core requirements for a gas sensor or catalytic converter remained the same, where the device should have both high sensitivity and good selectivity for gas sensor in order to detect trace amount of an explosive, hazardous or other critical gaseous chemicals against a complex dynamic background. The high sensitivity was guarantee a quick response to trigger the alert depending on preparation method[11], while the great selectivity was promoted the precision of that response. Also, the gas sensor should be reliable for long term utilization with maintained sensitivity and selectivity. Therefore, it required the sensing materials to have mechanical robustness and thermal stability.

---

\*Corresponding author: dr.issamiq@gmail.com

For a catalytic gas converter which is mounted on automobile especially, the point is to reduce or eliminate the usage of noble metals without sacrificing the conversion efficiency. On the other hand, it was expected to have the lower work temperature of catalytic converter for less energy consumption. Transparent conducting oxide (TCO) materials are good choice for gas sensor applications[12,13]. Recently, the high electrical conductivity of a TCO resulted from the presence of atomic-scale defects, which for n-type semiconductors, bring in donors that increase the electron population. The specific types of atomic-scale defects for a given TCO depend on the specific oxide and its synthesis. They may include oxygen vacancies, cation vacancies, oxygen interstitials, cation interstitials, impurity dopants, cation and anion anti-sites, and defect complexes, which consist of a combination of two or more point defects [14]. To synthesize  $\text{In}_2\text{O}_3$  and  $\text{SnO}_2$  films, many methods were adopted such as R.F. magnetron co-sputtering, thermal evaporation, chemical vapor deposition, laser pulse deposition, sol-gel, spray pyrolysis and spin coating technique [14,16]. ITO crystallizes cubic structure with lattice constant of  $a = 10.09 \text{ \AA}$ [17].

In this study, the growth of nanostructured thin films of  $\text{In}_2\text{O}_3$  and  $\text{In}_2\text{O}_3\text{-SnO}_2$  were reported using assistant microwave irradiation on seeded layer nucleated by spin coating method and this proposed preparation method which has never used a PVA- $\text{In}(\text{OH})_3\text{-Sn}(\text{OH})_4$  nanocomposite seed layer to synthesize Indium Tin Oxide nanostructures.

## 2. Materials and experimental method

Pure  $\text{In}_2\text{O}_3$  and  $\text{In}_2\text{O}_3\text{-SnO}_2$  thin films at ratio of Sn:In which is 20:80 wt/wt% were prepared by spin coating technique deposited onto silicon and glass substrates. Chemical solutions were prepared by mixing 0.1 M aqueous solutions of  $\text{InCl}_3$  and  $\text{SnCl}_4$  at the above ratios using a magnetic stirrer, then added to 1.5g PVA at  $80^\circ\text{C}$  for 2h, then the resultant solutions have been spin coated on substrates at 1500 rpm for 1min. This step was repeated several times to obtain the desired thickness for seed layer. Then 0.05 M of  $\text{InCl}_3$  and  $\text{SnCl}_4$  were mixed with 0.05 M of hexamine using magnetic stirrer for 1min prior the seeded substrates have been aligned vertically inside solution which were irradiated in microwave oven at 220W for 1h. Then washing the substrates with distilled water to remove any non-reacted materials, then dried in oven at  $100^\circ\text{C}$  for 30min. After that, the films were ready to be characterized. X-ray diffraction (XRD- 6000 Labx, supplied by Shimadzu, X-ray source is Cu) used to determine the structural properties. Atomic Force Microscope (AFM)-type (CSPM) used to analyze the film morphology.

## 3. Results and discussion

XRD used to investigate the structure of the prepared thin films. The plot between ( $2\theta$ ) versus diffracted ray intensity. The major diffraction peaks at  $2\theta = (30.2590, 35.4790 \text{ and } 51.2300)$ , for pure  $\text{In}_2\text{O}_3$ , thus the experimental results proved that the polycrystalline nature of the prepared sample as depicted in Fig. 1. The presence of tin oxide has been detected by observation peaks at  $2\theta = (26.2540, 33.8670, 37.9900 \text{ and } 51.8340)$ . The result corresponds with that described by H. A. Mohamed [17]. Moreover, a decrease in the main peak intensity is observed in the presence of tin oxide. A comparison with ASTM card (96-101-0589) and (96-210-4744), reveals that  $\text{In}_2\text{O}_3\text{-SnO}_2$  thin film exhibits a cubic crystal structure with a preferred orientation (222) for  $\text{In}_2\text{O}_3$  and (110) for  $\text{SnO}_2$ . The crystallite size ( $D$ ) is determined from main peak (222) and found to be equal to (18.9-14.5) nm as shown in Table (1) which based on Scherer formula which is:

$$(D = k\lambda / (\beta \cos\theta)) \quad (1)$$

where  $k$  is a correction factor=0.89,  $\beta$  is the full width at half maximum (FWHM) in radian and  $\theta$  is Bragg angle. When tin oxide addition, the phase of  $\text{SnO}_2$  appeared as shown in Fig. 1 with a preferred orientation (110) for  $\text{SnO}_2$  at  $2\theta=26.5263^\circ$  which intensity is higher than that for pure  $\text{In}_2\text{O}_3$ . It is clear that the addition ratios did not change the direction of crystalline growth of the

dominant planes (preferred orientation), where growth continues towards (222) direction for  $\text{In}_2\text{O}_3$ , which is attributable to the Drift model (Survival of the fastest) [18].

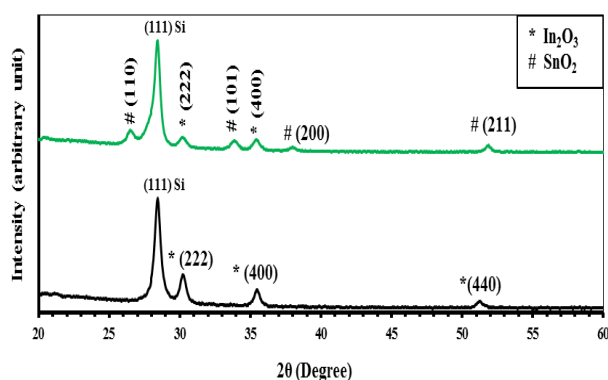


Fig. 1. X-ray diffraction patterns of ITO thin films.

An increase in the full width at half maximum (FWHM) and which consequently leads to a decrease in crystallite size, according to Scherer's formula equation after  $\text{SnO}_2$  addition as a comparison of pure Indium oxide thin film, which indicates that the deposited atoms of these films go towards nanostructure. There was a small shift toward a small angle of diffraction, (to the left of diagram), causing compression in the unit cell because of the ionic radius of the element Sn ( $0.69\text{\AA}$ ) smaller than that for In ( $0.80\text{\AA}$ ) [17], which leads to the atoms of Sn take up substitutional sites in order of Indium crystalline lattice.

Table 1. Average crystallite size ( $D$ ), inter planer spacing ( $d$ ) and FWHM for  $\text{In}_2\text{O}_3$  and  $\text{In}_2\text{O}_3\text{-SnO}_2$ .

% $\text{SnO}_2$	$2\theta$ (Deg.)	FWHM (Deg.)	$d_{hkl}$ Exp.( $\text{\AA}$ )	$D$ (nm)	hkl	$d_{hkl}$ Std.( $\text{\AA}$ )	Phase	Card No.
0	30.2590	0.4350	2.9513	18.9	(222)	2.9214	$\text{In}_2\text{O}_3$	96-101-0589
	35.4790	0.4844	2.5281	17.2	(400)	2.5300	$\text{In}_2\text{O}_3$	96-101-0589
	51.2300	0.4880	1.7818	18.1	(440)	1.7890	$\text{In}_2\text{O}_3$	96-101-0589
20	26.5240	0.6006	3.3578	13.6	(110)	3.3498	$\text{SnO}_2$	96-210-4744
	30.2330	0.5675	2.9538	14.5	(222)	2.9214	$\text{In}_2\text{O}_3$	96-101-0589
	33.8670	0.5643	2.6447	14.7	(101)	2.6439	$\text{SnO}_2$	96-210-4744
	35.4530	0.5678	2.5299	14.7	(400)	2.5300	$\text{In}_2\text{O}_3$	96-101-0589
	37.9985	0.5720	2.3661	14.7	(200)	2.3686	$\text{SnO}_2$	96-210-4744
	51.8340	0.6230	1.7624	14.2	(211)	1.7642	$\text{SnO}_2$	96-210-4744

Fig. 2 displays AFM image of  $\text{In}_2\text{O}_3$  and  $\text{In}_2\text{O}_3 - \text{SnO}_2$  the films. It shows the presence of homogenous grains throughout the film. The grain size of thin films is less than 100 nm. The grain size and film roughness ( $R$ ) increase after  $\text{SnO}_2$  addition as shown in Table 2. This property is ideal to improve gas sensitivity as shown later.

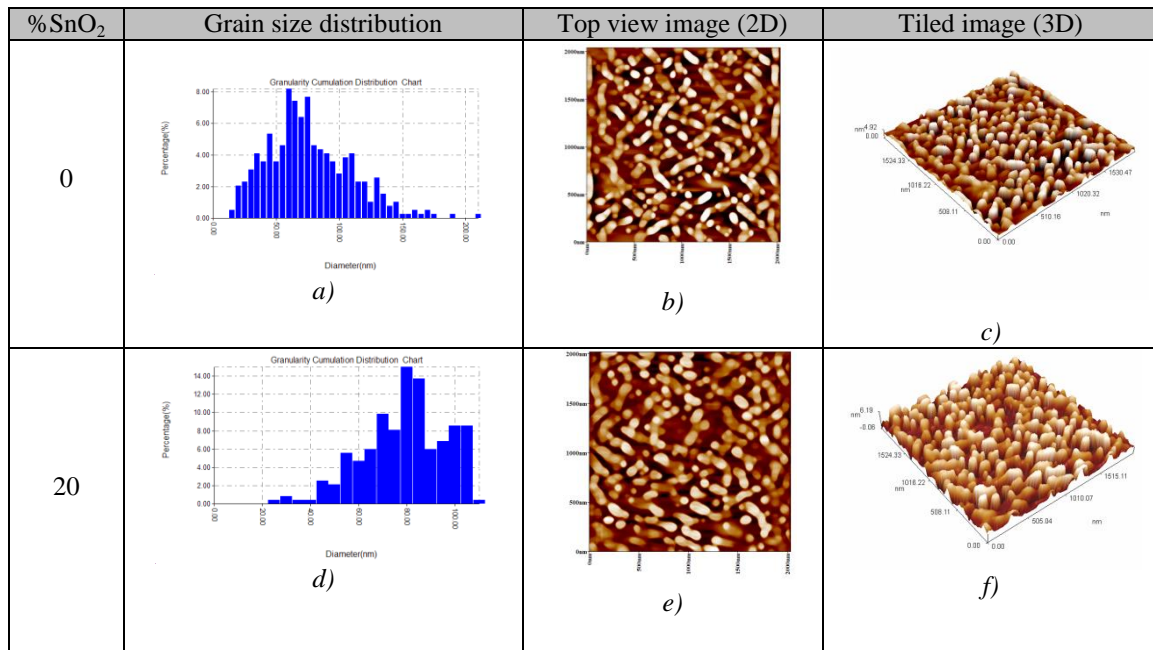


Fig. 2. The atomic force microscope analysis for In<sub>2</sub>O<sub>3</sub> and In<sub>2</sub>O<sub>3</sub>- SnO<sub>2</sub> films

Table 2. The average grain sizes and roughness average for In<sub>2</sub>O<sub>3</sub> and In<sub>2</sub>O<sub>3</sub>- SnO<sub>2</sub> films.

%SnO <sub>2</sub>	Average diameter (nm)	Roughness (nm)	Peak-Peak (nm)	(r.m.s.) nm
0	71.94	1.25	4.91	1.44
20	76.66	1.42	6.25	1.63

Thin films specimens are examined for gas sensing using NO<sub>2</sub> toxic gas with concentration of 50 ppm at different operation temperatures beginning from room temperature (25°C) up to 300°C with step of 100°C. The gas sensing property of the sensor is measured by collecting a change in resistance over two sensing electrodes under NO<sub>2</sub> gas. The change in the sensor resistance is attributed to ion adsorption of gas molecules, surface reaction of target gas with adsorbed oxygen on the surface of metal oxide [19]. Adsorbed ions are responsible for a change in conductivity. The negative charged ions are responsible for absorbing electrons and upward band bending around the edge of the grain. By absorbing oxygen molecules on the surface of metal oxide, they extract electrons from the conduction band E<sub>c</sub> and electrons trap at the surface in form of ions. This mechanism causes a band bending and the electron depleted region near the surface of each grain [20]. During the adsorption process at elevated temperatures, different oxygen species are formed on the surface of sensor thin film as O<sub>2</sub><sup>-</sup> and O<sup>-</sup> [19].

Some factors are important for studying sensing properties such as sensitivity, selectivity response time and recovery time.

The sensitivity factor (S%) for n-type semiconductors and by applying oxidizing gas is calculated using the following equation[21]:

$$S = |(R_a - R_g) / R_a| * 100\% \quad (2)$$

where S is the sensitivity, R<sub>a</sub> and R<sub>g</sub> are the electrical resistance of the film in the air and electrical resistance of the film in the presence of gas, respectively.

The response time of a gas sensor for n-type semiconductor material is defined as the time which sensor needs to reach 90% of minimum value of conductance upon introduction of the

oxidizing gas. Similarly, the recovery time is defined as the time required to recover to within 10% of the original baseline when the flow of oxidizing gas is removed [22].

Fig. 3 shows the variation of sensitivity as a function of time with on/off gas valve for  $\text{In}_2\text{O}_3$  at  $300^\circ\text{C}$  where there is no sensing for temperature less than  $300^\circ\text{C}$ . The sensing mechanism of  $\text{In}_2\text{O}_3$  is related to the ion sorption of gas species over the surface, leading to charge transfer between the gas and surface molecules and changes in the electrical conductance [21].

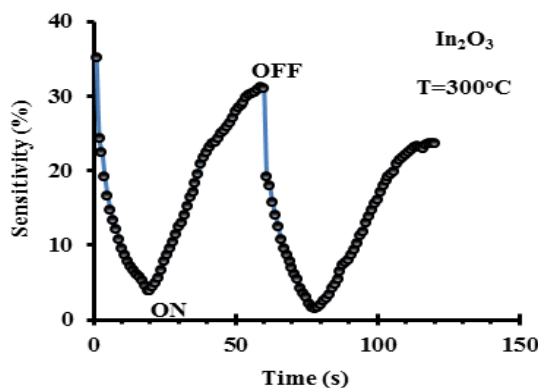


Fig. 3. The variation of sensitivity with time for Pure  $\text{In}_2\text{O}_3$  film against  $\text{NO}_2$  gas.

This figure shows increasing in the resistance value when the film was exposed to  $\text{NO}_2$  gas, (Gas on), then the resistance value back downward at the closure of the gas (Gas off). The reason for this behavior can be attributed to the following:  $\text{In}_2\text{O}_3$  is n-type and the electrons mainly participate in conductivity, when oxidizing gas enters, it takes electron from the material surface which leads to decrease electrons in material and decrease conductivity and increase the resistivity. In another word,  $\text{NO}_2$  gas undergoes an ionic reaction with the surface adsorption oxygen, where the electron on the oxygen, is extracted from the semiconductor and causes the conductivity of the  $\text{In}_2\text{O}_3$  materials to decrease, thus causing the resistance to increase.

After adding  $\text{SnO}_2$  the sensitivity improved significantly which may makes as catalyst for enhancing the reaction of gas molecules with oxide surface.

The changing in the resistance value according to the metal oxide semiconductor sensor is, in air, oxygen adsorbs on the surface and dissociates to form  $\text{O}^-$ , where the electron on the oxygen, is extracted from the semiconductor. This electron extraction tends to increase the resistance for the kind of n-type semiconductor where the majority charge carriers are electrons.

The operating temperature is defined as the temperature at which the resistance of the sensor reaches a constant value. Figure 4 represents the variation of sensitivity for  $\text{In}_2\text{O}_3$ - $\text{SnO}_2$  film against  $\text{NO}_2$  gas at different operating temperatures.

Results show that the sensitivity of  $\text{In}_2\text{O}_3$  -  $\text{SnO}_2$  films increase with increasing of the operating temperature at ( $200^\circ\text{C}$ ) and then decreases. It is obvious in table an increase in the operating temperature leads to an improvement of the films sensitivity which is attributed to increase in the rate of surface reaction of the target gas, then there was decreasing in sensitivity with increase of the operating temperature. Maximum point values for  $\text{In}_2\text{O}_3$  -  $\text{SnO}_2$  film which was seen at temperature of ( $200^\circ\text{C}$ ) which called optimal temperature as seen in Table 3. At the optimal temperature, the activation energy may be enough to complete the chemical reaction. There is an increase and decrease in the sensitivity indicates the adsorption and desorption phenomenon of the gas.

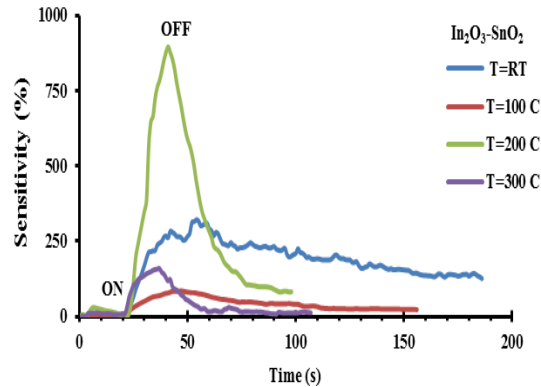


Fig. 4. The variation of sensitivity with time for  $\text{In}_2\text{O}_3\text{-SnO}_2$  film against  $\text{NO}_2$  gas at different operating temperatures.

The variation of sensitivity for  $\text{In}_2\text{O}_3\text{-SnO}_2$  film against  $\text{NO}_2$  gas at different operating temperatures is shown in Fig. 5. One can observe that there is a selectivity at  $200^\circ\text{C}$ .

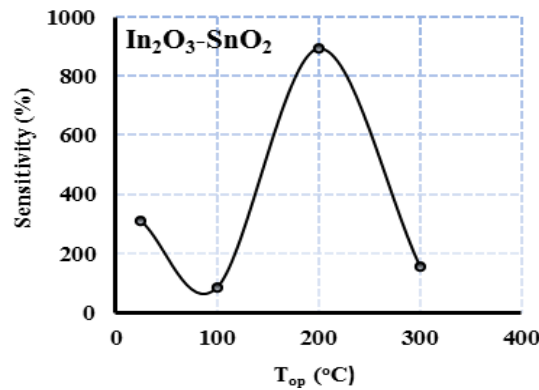


Fig. 5. The variation of sensitivity with operating temperature for  $\text{In}_2\text{O}_3\text{-SnO}_2$  film against  $\text{NO}_2$  gas.

The sensitivity as well as response time depend on operating temperature since the chemical kinetics in solid-gas reaction is governing by the dependence of temperature [17]. The response speed is studied with operating temperature as well as at which the sensor exhibited a maximum sensitivity at ( $200^\circ\text{C}$ ) as illustrated in figure (6) which shows the relation between the response time and the recovery time at different operating temperatures of  $\text{In}_2\text{O}_3\text{-SnO}_2$  thin film. One can observe that there is fast response with increasing operating temperature as shown in Table (3).

The quick response sensor for  $\text{NO}_2$  gas may due to faster oxidation of gas [23], in addition, it can be attributed to the increasing in oxygen vacancies created upon  $\text{In}_2\text{O}_3$  lattice. Besides that, ions of  $\text{Sn}^{+4}$  occupy energy level above valance band and behave as an activator, consequently holes easily move to valance band, and increased the adsorption of oxygen on the surface extracts valance holes from the near surface region forming holes depleted surface layer, and this increasing number of active adsorption sites achieved fast response time for sensor [24].

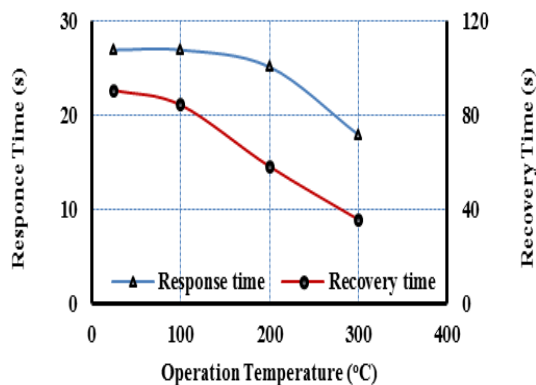


Fig. 6. The variation of Response time and Recovery time for  $\text{In}_2\text{O}_3\text{-SnO}_2$  film against  $\text{NO}_2$  gas.

Table 3. Sensitivity, response and recovery times as a function of operating temperature for  $\text{In}_2\text{O}_3$  and  $\text{In}_2\text{O}_3\text{-SnO}_2$  against  $\text{NO}_2$  toxic gas.

$T_{op}$ . (°C)	$\text{In}_2\text{O}_3$			$\text{In}_2\text{O}_3\text{-SnO}_2$		
	S%	$T_{res}$ (s)	$T_{rec}$ (s)	S%	$T_{res}$ (s)	$T_{rec}$ (s)
25	----	----	----	312	21.6	106.2
100	----	----	----	87	23.4	66.6
200	----	----	----	895	16.2	44.1
300	21.5	18	38	158	14.4	29.7

The changing of sensitivity is just only influenced by the presence of amount of some gases of interest [24]. A competition results between the oxygen removing the electrons and the combustible gas restoring these electrons. So, the steady state value of resistance of the metal oxide depends on the concentration of the combustible gas and this is illustrated in Figure 7 (a and b) and the Table 4 shows the sensitivity as a function of  $\text{NO}_2$  gas concentration for  $\text{In}_2\text{O}_3\text{-SnO}_2$  which is deposited on silicon substrates at operating temperature of  $200^\circ\text{C}$ .

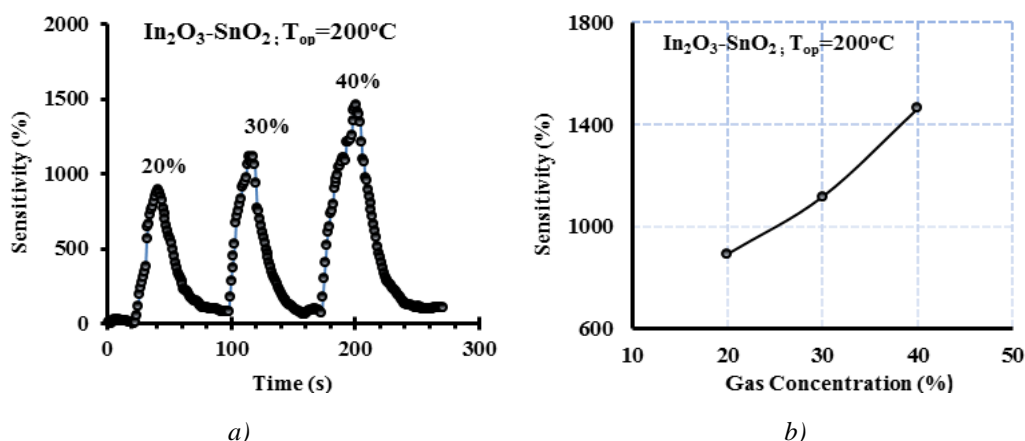


Fig. 7. (a) The variation of sensitivity with time at  $200^\circ\text{C}$  operating temperature for  $\text{In}_2\text{O}_3\text{-SnO}_2$  film against different concentrations of  $\text{NO}_2$  gas; (b)  $\text{NO}_2$  concentrations dependence of S%.

Table 4. Sensitivity for  $\text{In}_2\text{O}_3\text{-SnO}_2$  at  $T_{op}$ . of  $200^\circ\text{C}$  as a function of  $\text{NO}_2$  toxic gas concentration.

% concentration of $\text{NO}_2$	20	30	40
% S	895	1119	1464

#### 4. Conclusions

In<sub>2</sub>O<sub>3</sub>-SnO<sub>2</sub> thin films were prepared by assistance of microwave irradiation on seeded layer prepared by spin coating method. The X-ray diffraction shows the polycrystalline nature of deposited films with cubic structure. The crystallite size of the film was calculated using Debye-Scherrer formula is from 18.9 nm for In<sub>2</sub>O<sub>3</sub> and 14.5 nm for In<sub>2</sub>O<sub>3</sub>-SnO<sub>2</sub>. The AFM images show nano size of the prepared films with increasing roughness from 1.25 to 1.42 nm that is good property for improving gas sensing which has more than 800 % after addition SnO<sub>2</sub> to In<sub>2</sub>O<sub>3</sub> lattice with fast response and recovery time.

#### References

- [1] G. Neri, Recent patents on Materials Science **4**, 146(2011).
- [2] I. K. Jasim, I. M. Ibrahim, M. K. Alyas, Iraqi J. Sci. **59**(1A) 76 (2018).
- [3] S. A. Hamdan, I. M. Ali, Baghdad Sci. J. **16**, 1 (2019).
- [4] N. Yamazoe, Sens. Actuat. B Chem. **108**, 2 (2005).
- [5] C.Y. Cao, J. Qu, W.S. Yan, J. F. Zhu, Z.Y. Wu, W. G. Song, *Langmuir* **28**, 4573 (2012).
- [6] H. Li, W. Li, Y. Zhang, T. Wang, B. Wang, W. Xu, J. Mater. Chem. **21**, 7878 (2011).
- [7] O. A. Sadik, A. K. Wanekaya, S. Andreescu, J. Environ. Monit. **6**, 513 (2004).
- [8] K. Kawamura, K. Kerman, M. Fujihara, N. Nagatani, T. Hashiba, E. Tamiya, Sens. Actuat. B Chem. **105**, 495 (2005).
- [9] A. M. Ruiz, G. Sakai, A. Cornet, K. Shimanoe, J. R. Morante, N. Yamazoe, Sens. Actuat. B Chem. **93**, 509 (2003).
- [10] I. F. Akyildiz, I. H. Kasimoglu, Ad Hoc. Netw. **2**, 351 (2004).
- [11] S. A. Khalaf, I. M. Ali, Iraqi J. Sci. **59**(4C) 2242 (2018).
- [12] I. M. Ibrahim, J. A. Najim, A. M. Rakea, Iraqi J. Physics, **15**(35) 64 (2017).
- [13] S. Sh. hamd, A. Ramizy, I. M. Ibrahim, J. Kufa-Physics, **9**(2) 10 (2017).
- [14] V. Sivaranjani, P. Philominathan, Int. J. Thin. Fil. Sci. Tec. **4**(3), 219 (2015).
- [15] B. J. Chen, X. W. Sun, B. X. Tay, Mater. Sci. Eng. B **106**, 300 (2004).
- [16] J. B. Choi, J. H. Kim, K. A. Jeon, S. Y. Lee, Mater. Sci. Eng. B **102**, 376 (2003).
- [17] H. A. Mohamed, Int. J. Physical Sciences **7**(13), 2102 (2012).
- [18] V. Kachkanov, B. Leung, J. Song, Y. Zhang, C. Tsai, G. Yuan, J. Han, K. O'Donnell, Scientific Reports **4**, Article number: 4651, 2014.
- [19] D. Cappus, M. HaBel, E. Neuhaus, M. Heber, F. Rohr, H.-J. Freund, Surface Science **337**, 268 (1995).
- [20] J. C. Shoou, W. Y. Weng, C. L. Hsueh, T. J. Hsueh, Nano Communication Networks **1**(4), 283 (2010).
- [21] T. Sujitno, S. Sudjatmoko, Atom Indones. **2**, 2011.
- [22] A. Z. Sadek, W. Wlodarski, K. Kalantar-Zadeh, S. Choopun, Proc. IEEE Sensors **2**, 1326 (2005).
- [23] D. Kohl, Sensors and Actuators **18**(1), 71 (1989).
- [24] S. A. Garde, Sensors & Transducers Journal **11**, 128 (2010).